JOURNAL OF MATERIALS SCIENCE 33 (1998) 549–558

Perovskite-type $BaTiO_3$ ceramics containing particulate SiC

Part II *Microstructure and mechanical properties*

H.J. HWANG*, K. NIIHARA
The Institute of Scientific and Industrial Research, Osaka University, 8-1 Mihogaoka, Ibaraki, Osaka 567, Japan

Microstructure and mechanical properties of $BaTiO_3$ and $BaTiO_3$-based composites containing nanosized SiC particulates were investigated. Fracture behaviour and fractography were also discussed from the fracture surface observation by scanning electron microscopy and by the controlled surface flaw method. The added SiC particulates were uniformly distributed within the matrix $BaTiO_3$ grains, with some larger particulates located at the $BaTiO_3$ grain boundaries. The microstructure of $BaTiO_3$ was modified by incorporation of the SiC particulate. Mechanical properties, particularly the fracture strength, were remarkably improved by adding the SiC particulate, owing to grain-size reduction and/or crystal structure change by incorporating the SiC. From the fracture surface observations, it was confirmed that the subcritical crack growth phenomenon of $BaTiO_3$ was also improved by the nanosized SiC dispersions.

1. Introduction

$BaTiO_3$-based ferroelectrics transform from the paraelectric cubic phase to ferroelectric tetragonal phase at the Curie temperature, (T_c). This transformation causes a complicated stress system in the ferroelectric material, and then results in the generation of internal stress and mechanically twined microstructure at room temperature. This complicated behaviour yields useful information for understanding the processing–microstructure–property relationships of ceramics [1–3]. Thus, mechanical properties and fractography of ferroelectric and piezoelectric materials have been studied, together with the electrical properties [4–9]. Polhanka *et al.* [10, 11] indicated that the internal stress resulting from the paraelectric to ferroelectric phase transformation occurring in $BaTiO_3$-based ceramics during cooling through T_c after the sintering process can measurably decrease their fracture strength. Bruce *et al.* [12] investigated the subcritical crack growth (SCG) phenomenon of $Pb(Zr, Ti)O_3$-(PZT) ceramics.

Recently, electrical devices have been miniaturized and are used under quite severe atmospheres. $BaTiO_3$-based ceremics with high mechanical properties and reliability are, therefore, strongly required, as are stable dielectric properties. However, comprehensive investigations on the relationship between the microstructure and mechanical properties of $BaTiO_3$-based ceramics are somewhat lacking [13, 14]. In Part I of this paper, new types of $BaTiO_3$-based composites with nanosized SiC particulates as a dispersive phase, were successfully fabricated by hot pressing, and their crystal structure was investigated [15]. In the present study, the effects of the SiC particulates on the microstructure evolution and mechanical properties were investigated.

Fracture behaviour and fractography were also discussed from the fracture surface observation by scanning electron microscopy and by a controlled surface flaw (CSF) method.

2. Experimental procedure

$BaTiO_3$-based composites with SiC particulate were prepared using a conventional method for the fabrication of ceramics. The starting materials were $BaTiO_3$ and β–SiC powders. The Ba/Ti atomic ratio of the starting $BaTiO_3$ powder was 0.999 and the crystal phase was cubic. Characteristic properties of starting powders and details of the fabrication procedure were described in Part I [15]. Sintered specimens were cut with a diamond cutting machine. The section surface was polished with diamond paste for various evaluations and observations, as will be mentioned later.

The bulk density was determined by Archimedes' method in toluene. The X-ray diffraction pattern was taken using nickel-filtered CuK_α radiation. The grain size of the specimens were determined using a linear

* *Present address*: National Industrial Research Institute of Nagoya, 1-1 Hirate-cho, Kita-ku, Nagoya 462, Japan

0022–2461

intercept method: the average linear intercept, L was measured, and L ($\pi/2$) was taken to be the average grain size, G.

For Young's modulus measurement, a resonance vibration method was used at about 2 kHz frequency [15]. Shear modulus was measured using an inverted torsion pendulum method at frequencies ranging from 1–20 Hz in the temperature range -196 to 200 °C in nitrogen. Fracture strength was measured on polished (0.5 μm) bar-shaped specimen (3 mm × 4 mm × 40 mm) using a three-point bending method at a crosshead speed of 0.5 mm min^{-1}. Fracture toughness was measured using a micro-indentation technique using a micro-Vickers diamond indentor and the controlled surface flaw (CSF) method at room temperature [16]. For the former method, an indentation load of 9.8 N was applied for 15 s. For the latter method, the polished specimens were indented with a Knoop indentor at load levels of 9.8, 19.6, 49, 98 and 196 N, and then were broken using a three-point bending fixture. Prior to the bending test, the indented surfaces were ground and polished to 50 μm to remove any possible surface-stressed layer caused by the indentation. The bending test was performed using an Instron Universal Testing machine at a constant crosshead speed of 0.5 mm min^{-1}. For all specimens, the fracture initiated at the site of the controlled surface flaw. Fracture surface and domain structure were observed by scanning electron microscopy (SEM) and transmission electron microscopy (TEM), respectively.

3. Results

3.1. Microstructure

X-ray diffraction analysis showed $BaTiO_3$–SiC composites sintered at 1300 °C were mainly composed of $BaTiO_3$ and β–SiC. Up to 5 vol% particulate SiC addition produced no additional phases, such as $Ba_4Ti_{13}O_{30}$, $Ba_6Ti_{17}O_{30}$, nor $BaTiO_3$–xBaO compounds [15].

Fig. 1 shows the densification behaviour of the monolithic $BaTiO_3$ and $BaTiO_3$–SiC composites with different SiC contents. The relative density markedly depended on the sintering temperature, and especially for the composites with 3 and 5 vol% SiC, it increased abruptly with increasing sintering temperature, as is evident in Fig. 1. Nearly full density was achieved by sintering at a temperature as low as 1200 °C for the monolithic $BaTiO_3$. The incorporation of the SiC particulate had a tremendous effect on the densification rate. The highest density (99% theoretical density) was obtained for $BaTiO_3$–1 vol% SiC when the sintering temperature was raised to 1300 °C. At a higher SiC, content, however, the density gradually decreased as the SiC content increased, and the maximum relative density was lowered to 97% and 96% for $BaTiO_3$–3 vol% SiC and 5 vol% SiC composites sintered at 1300 °C, respectively. There was no remarkable change when the sintering temperature was raised to 1350 °C.

Fig. 2a and b show the dispersion states of the added SiC particulates. A transmission electron micrograph, indicating the lattice fringe images of the interface between the matrix grain and SiC, is shown in Fig. 2c. It seems that the grain-boundary movement is depressed by the SiC particulates, as can be seen in Fig. 2a. This may be caused by the grain-boundary pinning force of SiC, pointed out by other researchers [17]. The SiC particulates less than about 10 nm in size were uniformly distributed within the matrix $BaTiO_3$ grains, with some larger particulates located at the $BaTiO_3$ grain boundaries. The intragranular SiC particulates appear to result from the break-away of the grain boundary from the pinning force, like the pores trapped within matrix grains [18, 19]. In addition, no reaction phases were found between $BaTiO_3$ matrix and SiC particulates incorporated within the matrix $BaTiO_3$ grains, nor at matrix grain boundaries and/or three-grain junctions.

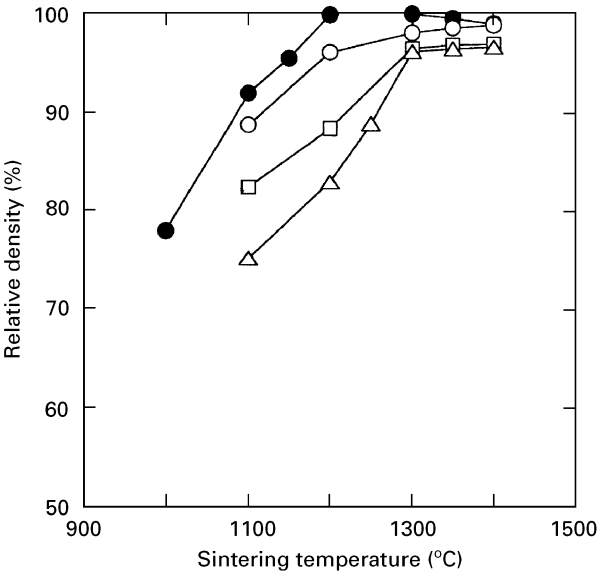

Figure 1 Relative density change with respect to the sintering temperature for $BaTiO_3$ and $BaTiO_3$–SiC composites. SiC content (vol %) : (●) 0, (○) 1, (□) 3, (△) 5.

Fig. 3 shows typical scanning electron micrographs of the thermally etched surfaces for the monolithic $BaTiO_3$ sintered at each temperature for 1 h. Fine-grained $BaTiO_3$, having a uniform grain size of 1–2 μm, was observed after sintering at 1200 °C, and the grain size was almost constant when the sintering temperature was below 1300 °C. However, the grains started to grow abnormally when the sintering temperature was raised to 1320 °C. The bimodal grain structure with small grains of 2–4 μm and large grains over 100 μm was observed upto the sintering temperature of 1400 °C. Thereafter, the grain structure was nearly saturated with the uniform and large grains of 100 μm for the specimen sintered at 1450 °C for 1 h. A fact to be noticed in Fig. 3 is that the spontaneous cracking begins to appear primarily along grain boundaries for the specimen sintered at 1350 °C for 1 h. In general, spontaneous cracking of polycrystalline ceramics results from the internal stresses between grains, owing to incompatible strains from either thermal expansion anisotropy or phase transformation

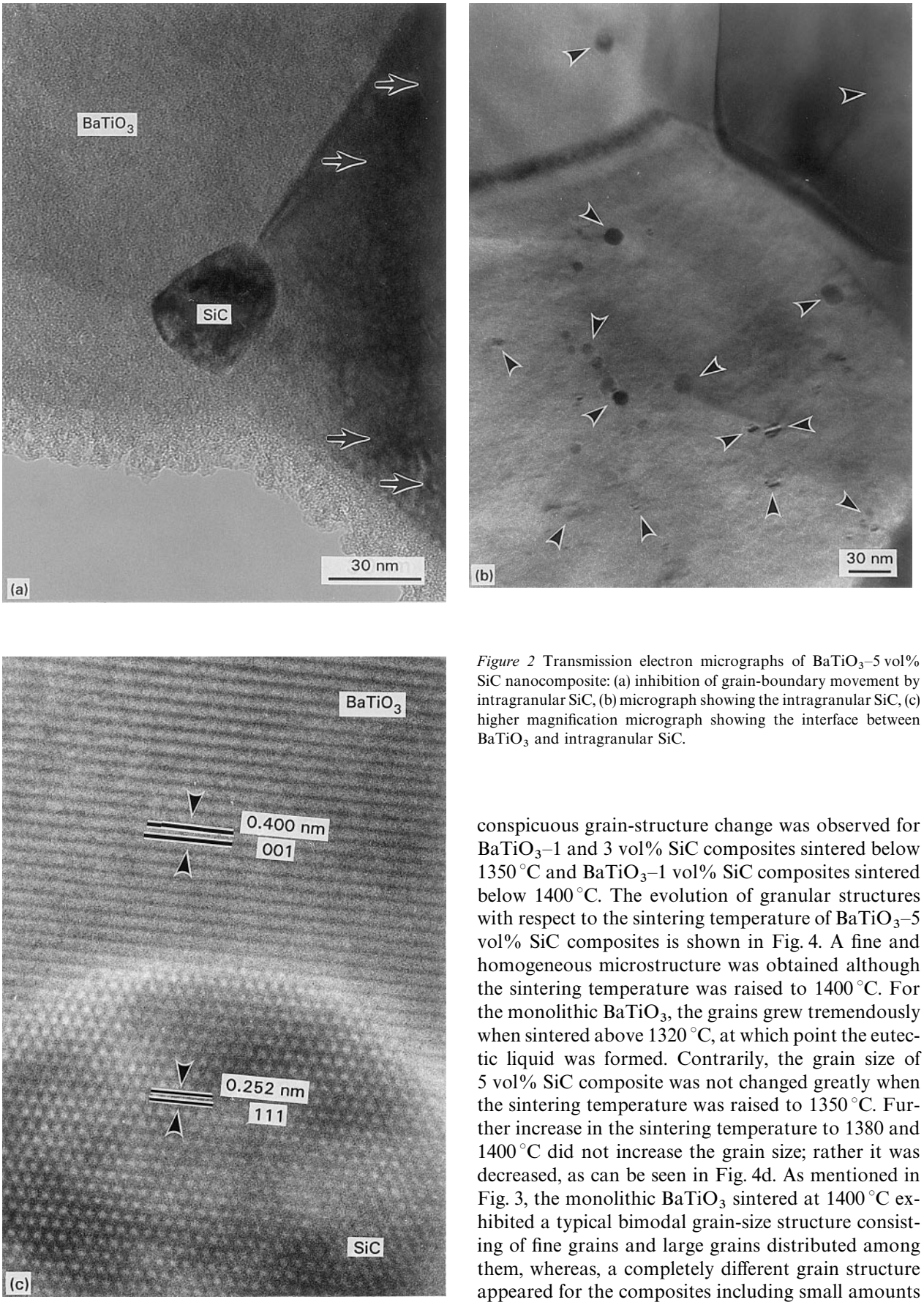

Figure 2 Transmission electron micrographs of $BaTiO_3$–5 vol% SiC nanocomposite: (a) inhibition of grain-boundary movement by intragranular SiC, (b) micrograph showing the intragranular SiC, (c) higher magnification micrograph showing the interface between $BaTiO_3$ and intragranular SiC.

[20]. The spontaneous cracking observed in the present study must be caused by the paraelectric to ferroelectric phase transformation.

In comparison with the grain-structure change with sintering temperature for the monolithic $BaTiO_3$, no conspicuous grain-structure change was observed for $BaTiO_3$–1 and 3 vol% SiC composites sintered below 1350 °C and $BaTiO_3$–1 vol% SiC composites sintered below 1400 °C. The evolution of granular structures with respect to the sintering temperature of $BaTiO_3$–5 vol% SiC composites is shown in Fig. 4. A fine and homogeneous microstructure was obtained although the sintering temperature was raised to 1400 °C. For the monolithic $BaTiO_3$, the grains grew tremendously when sintered above 1320 °C, at which point the eutectic liquid was formed. Contrarily, the grain size of 5 vol% SiC composite was not changed greatly when the sintering temperature was raised to 1350 °C. Further increase in the sintering temperature to 1380 and 1400 °C did not increase the grain size; rather it was decreased, as can be seen in Fig. 4d. As mentioned in Fig. 3, the monolithic $BaTiO_3$ sintered at 1400 °C exhibited a typical bimodal grain-size structure consisting of fine grains and large grains distributed among them, whereas, a completely different grain structure appeared for the composites including small amounts of SiC, as shown in Fig. 5. It was observed that the grains grew abruptly to a size of above 300 μm for 1 vol % SiC when the sintering temperature was raised to 1400 °C. Small grains of 2–3 μm were also observed between the large grains, and the fracture mode of small grains was intergranular, as can be seen in Fig. 5b. This observation suggested that a weak

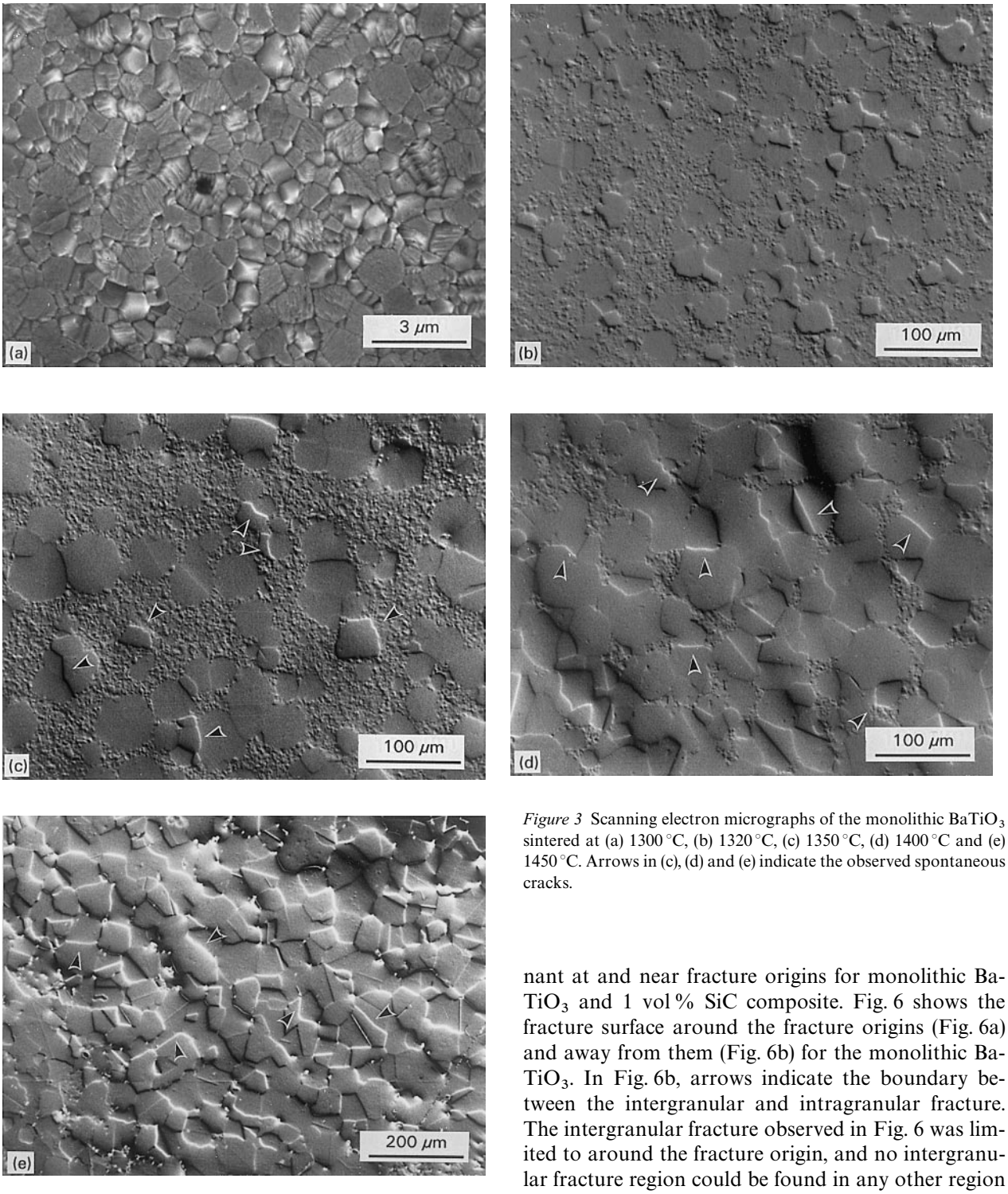

Figure 3 Scanning electron micrographs of the monolithic $BaTiO_3$ sintered at (a) 1300 °C, (b) 1320 °C, (c) 1350 °C, (d) 1400 °C and (e) 1450 °C. Arrows in (c), (d) and (e) indicate the observed spontaneous cracks.

grain-boundary phase existed between small grains. For the higher SiC additions of 3 and 5 vol %, the morphology of the grain structure was restored to typical $BaTiO_3$ grain structure sintered at 1300 °C. The change in the grain size with sintering temperature and SiC content is summarized in Table I, together with some mechanical properties.

Generally, the fracture mode of pure $BaTiO_3$-based ceramics is known to be intragranular [21]. In the present study, the fracture mode was also intragranular, regardless of the sintering temperature and the SiC dispersion. On the other hand, further observations revealed that the intergranular fracture was predominant at and near fracture origins for monolithic $BaTiO_3$ and 1 vol % SiC composite. Fig. 6 shows the fracture surface around the fracture origins (Fig. 6a) and away from them (Fig. 6b) for the monolithic $BaTiO_3$. In Fig. 6b, arrows indicate the boundary between the intergranular and intragranular fracture. The intergranular fracture observed in Fig. 6 was limited to around the fracture origin, and no intergranular fracture region could be found in any other region of the fracture surface. Thus, it is suggested that the intergranular fracture occurred before the brittle (catastrophic) fracture for monolithic $BaTiO_3$. A similar observation was also made for the $BaTiO_3$–1 vol % SiC composite.

3.2. Mechanical properties

Fig. 7 shows fracture-strength variation with sintering temperature for $BaTiO_3$ and $BaTiO_3$–SiC composites. By incorporating small amounts of SiC, the fracture strength improved markedly compared with that of monolithic $BaTiO_3$. Of the specimens sintered at 1250 °C, for example, the fracture strength at 1 vol % SiC was twice that of monolithic $BaTiO_3$. The

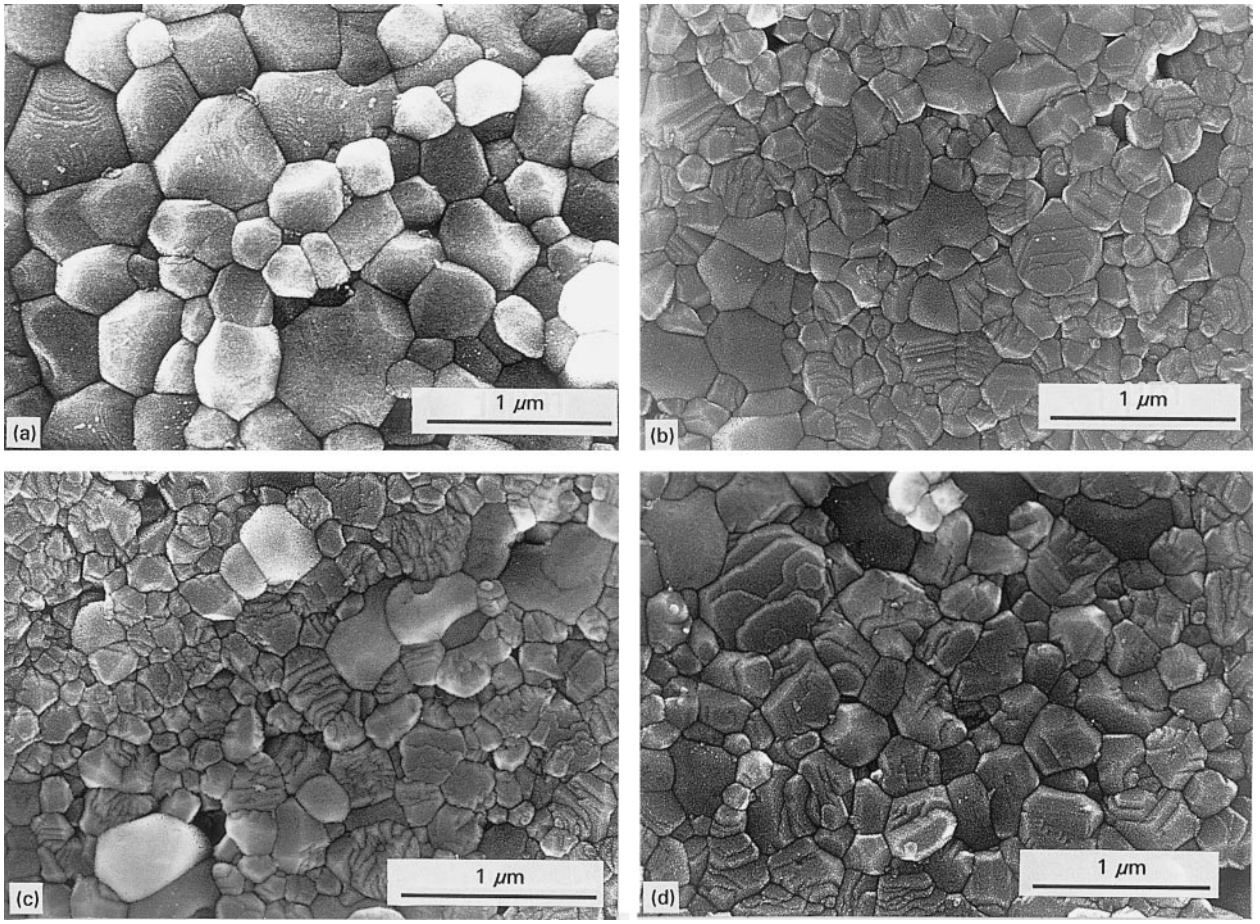

Figure 4 Scanning electron micrographs of $BaTiO_3$–5 vol% SiC sintered at (a) 1300 °C, (b) 1350 °C, (c) 1380 °C and (d) 1400 °C.

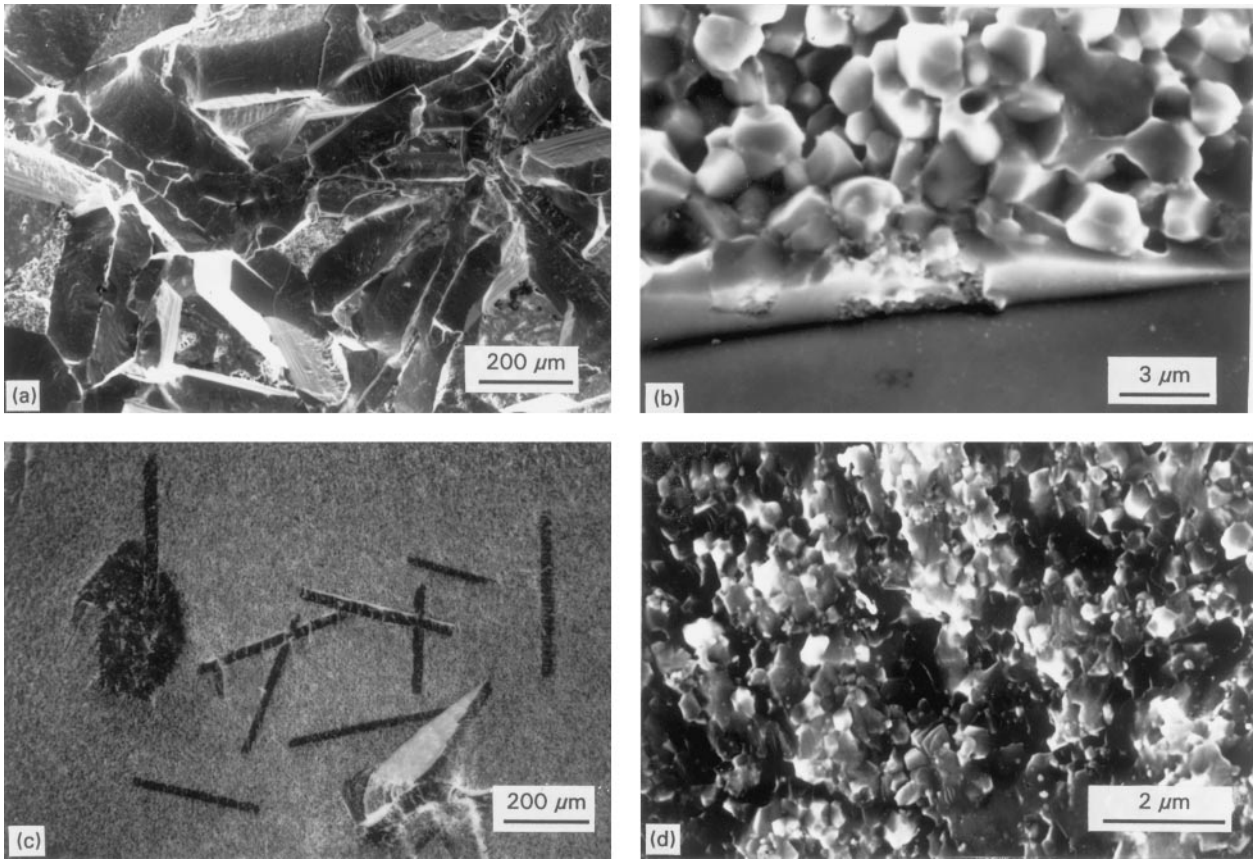

Figure 5 Typical fracture surfaces showing the abnormal grain growth for (a, b) $BaTiO_3$–1 vol% SiC composite and (c, d) 3 vol% SiC composite sintered at 1400 °C in an argon atmosphere.

TABLE I Some properties of $BaTiO_3$ and $BaTiO_3$–SiC composites

SiC content (vol %)	Sintering temp. (°C)	Crystal structure[a]	Relative density (%)	Grain size (μm)	Vickers hardness (GPa)	Young's modulus (GPa)	Fracture toughness (MPa $m^{1/2}$)	Fracture strength (MPa)
0	1300	Tetra	99.9	1.35	6.96	94	0.86	174
	1320	Tetra	99.9	2.5/45.2[b]	6.70	–	–	101
	1400	Tetra	99.0	13.5/107[b]	–	–	–	99
	1450	Tetra	98.4	123	–	–	–	46
1	1300	Tetra	98.0	0.84	7.67	129	0.99	282
	1350	Tetra	98.6	1.18	7.30	–	–	301
	1400	Hexa, tetra	98.9	2.8/304*	–	–	–	69
3	1300	P-cubic	96.2	0.48	9.15	141.2	1.22	350
	1350	P-cubic	96.9	0.66	8.98	–	–	291
	1400	P-cubic, hexa	97.0	1.3/189*	–	–	–	107
5	1300	P-cubic	95.8	0.35	9.23	141.4	1.19	305
	1350	P-cubic	96.1	0.32	9.18	–	–	315
	1400	P-cubic	96.3	0.40	–	–	–	302
	1450	P-cubic	96.5	–	–	–	–	249

[a] Tetra, tetragonal; P-cubic, pseudo-cubic; hexa, hexagonal; hexa, tetra, major phase is hexagonal.
[b] Bimodal distribution.

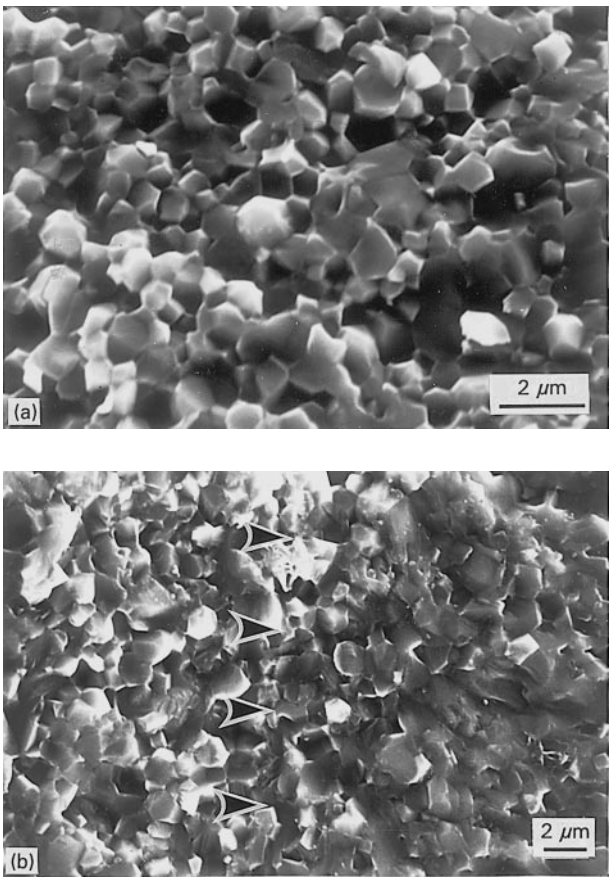

Figure 6 Typical scanning electron micrographs of fracture surfaces for the monolithic $BaTiO_3$ (a) around the fracture origins, and (b) away from them.

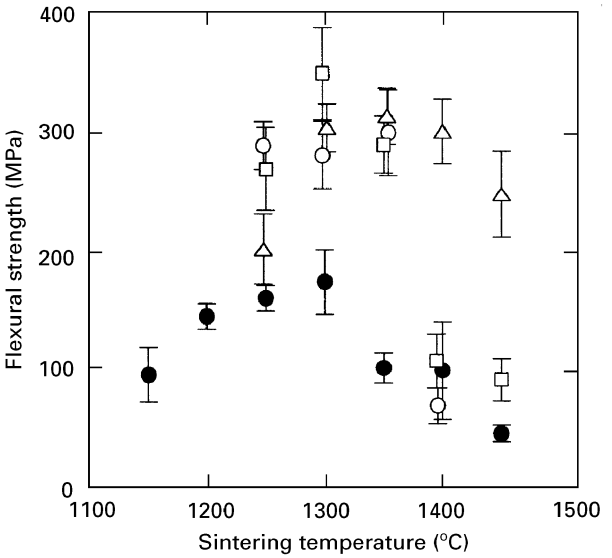

Figure 7 Flexural strength change with sintering temperature for $BaTiO_3$ and $BaTiO_3$–SiC composites. SiC content (vol %); (●)0, (○)1, (□)3, (△)5.

maximum fracture strength (350 MPa) was observed for 3 vol % SiC composite sintered at 1300 °C for 1 h.

As can be seen from Fig. 7, with increasing sintering temperature, the fracture strength first increased, and reached maximum value at approximately 1300 °C for the monolithic $BaTiO_3$. Thereafter, the fracture strength began to decrease gradually. The fracture strength of $BaTiO_3$–SiC composites also changed with sintering temperature, as for the monolithic $BaTiO_3$. This temperature dependence of the fracture strength must be associated with the relative density and grain growth, described in Figs 1 and 5.

The variation of fracture strength with crystal structure is shown in Fig. 8 for $BaTiO_3$–SiC composites sintered at 1350 °C. The fracture-strength measurement was carried out at 25 °C below T_c and at 150 °C above this temperature in air. Similarly, with the monolithic $BaTiO_3$ [10, 11], the fracture strength of composites was higher in the paraelectric state than that in the ferroelectric state, and this is probably due to the existence of local tensile stresses resulting from the paraelectric to ferroelectric phase transformation. This observed fracture-strength difference reached a maximum value of 120 MPa for 1 vol % SiC, and thereafter it decreased gradually with SiC

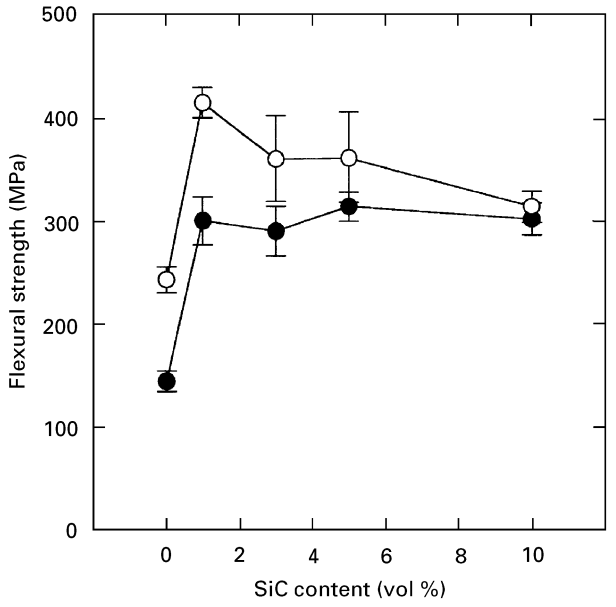

Figure 8 Flexural strength change with SiC content for $BaTiO_3$ and $BaTiO_3$–SiC composites. Measurements were made at (●) 25 °C (ferroelectric phase) and (○) 150 °C (paraelectric phase).

content, and finally became nearly zero for 10 vol % SiC composite.

As summarized in Table I, the monolithic $BaTiO_3$ remained in the ferroelectric tetragonal phase regardless of the sintering temperature. The crystal structure gradually changed from tetragonal to cubic phase with increasing SiC content. The crystal structure was pseudo-cubic for 3 and 5 vol % SiC composites sintered at 1300 °C, as reported in the Part I [15]. Hexagonal phase started to appear for 1 and 3 vol % SiC composites sintered at 1400 °C. The average grain size gradually decreased from about 2 μm (for the monolithic $BaTiO_3$) to less than 0.3 μm for 10 vol % SiC with increasing SiC content. The drastic reduction in grain size by the SiC incorporation indicates that SiC is very effective in controlling the grain structure of $BaTiO_3$ ceremics. Not only the microstructure but also mechanical properties, such as fracture toughness, micro-hardness and Young's modulus, were changed significantly by incorporating the SiC particulate. The fracture toughness increased with increasing SiC content. Micro-hardness and Young's modulus also increased when the SiC content was less than 3 vol %. The measured micro-hardness and Young's modulus values were much higher than those expected from the Rule of Mixtures.

Typical scanning electron micrographs of the fracture surfaces broken from Knoop impressions are shown in Fig. 9 for monolithic $BaTiO_3$, 1 and 5 vol % SiC and composites. Generally, the indentation fracture process appears to be a quasi-static and slow fracture situation, whereas the subsequent fracture from the initial flaw is fast and catastrophic. Thus, rate effects can lead to fracture morphology difference which might contribute to flaw visibility. In the present study, fortunately, a little difference in the fracture made it possible to distinguish the initial flaw from the fast fracture region to evaluate the fracture toughness by the CSF method. The semi-circular flaws produced by the Knoop indentation are well-defined, appearing bright against the darker fast-fracture surface. Moreover, as can be seen in Fig. 9a–d, the initial flaw was readily visible because a dark region was clearly observed between the initial flaw and the catastrophic fracture for the monolithic $BaTiO_3$ and $BaTiO_3$–1 vol% SiC composite. This dark region, which is thought to be the SCG region, became smaller with increasing SiC content, and finally disappeared for 5 vol % SiC composite.

4. Discussion

4.1. Microstructure

The abnormal grain growth and bimodal grain structure observed in Fig. 3b–e will be closely related to the formation of liquid phases. The sintering of $BaTiO_3$ ceramics is normally performed with a small excess of TiO_2 (the Ba/Ti atomic ratio is less than 1) as a sintering aid. It should be recalled that the excess TiO_2 reacts with $BaTiO_3$ to give $Ba_6Ti_{17}O_{40}$ which, with $BaTiO_3$ forms a eutectic melt at 1312 °C. The existence of the liquid phase during sintering, however, commonly not only promotes the sinterability but also gives rise to a pronounced discontinuous grain growth of $BaTiO_3$ [22]. In the present study, the temperature at which the abnormal grain growth begins to appear to correspond exactly to the liquid formation temperature of $Ba_6Ti_{17}O_{40}$. As the Ba/Ti atomic ratio of the starting $BaTiO_3$ powder in the present study was 0.999, an excess of 0.001 mol % TiO_2 excess exists. Although the amount of liquid phase is very small and not detected by X-ray diffraction analysis, it is apparent that the grain growth anomaly as seen in Fig. 3b–e is the result of the formation of the liquid phase.

The microstructure of $BaTiO_3$ was considerably modified by the incorporation of the SiC. As can be seen in Fig. 1, it is evident that the presence of the SiC particulates prevents the grain-boundary migration by the pinning force of SiC and limits the grain growth. So, the grain size of $BaTiO_3$ was significantly reduced as the SiC content increased, as summarized in Table I. Accordingly, fine-grained microstructure could be obtained when the sintering temperature was raised to 1400 °C for $BaTiO_3$–5 vol % SiC composite (see Fig. 4). On the other hand, the grain-size reduction with sintering temperature, observed in Fig. 4d, is not clear. For the monolithic $BaTiO_3$ sintered at above the liquid-formation temperature, it is well known that the microstructure is determined by the nucleation rate and growth rate of the nuclii [22]. If the fine SiC particulates can serve as nucleation sites for grain growth in the presence of the liquid phases, the decrease in the grain size can be explained somewhat. However, further investigation will be required.

The abnormal grain growth observed in $BaTio_3$–1 and 3 vol % SiC composites sintered at 1400 °C seems to be associated with the liquid-phase formation and hexagonal $BaTiO_3$ phase. X-ray diffraction analysis showed that a small amount of $Ba_2TiSi_2O_8$ phase was detected for the composites sintered at 1400 °C [15].

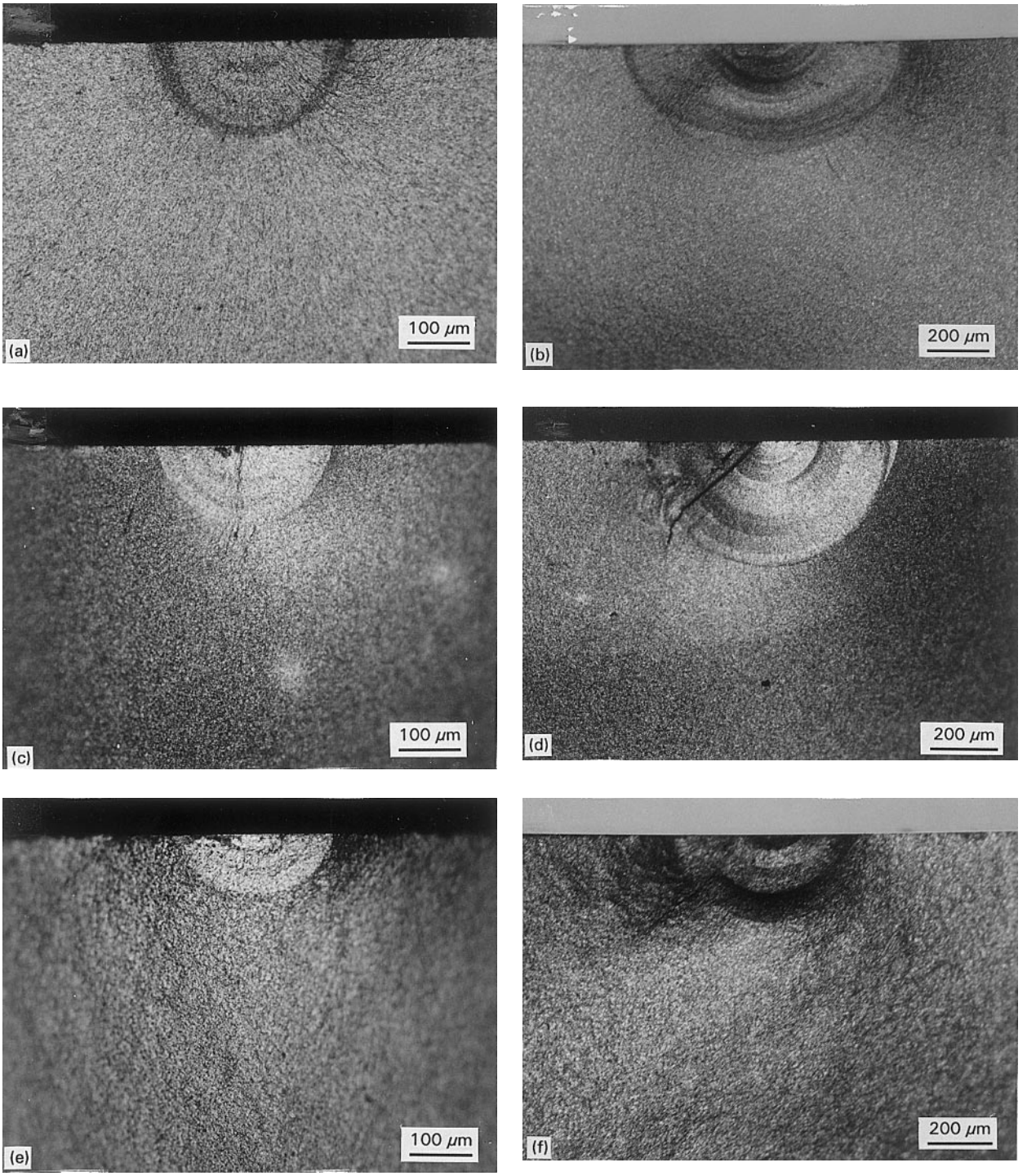

Figure 9 Optical photographs of fracture surfaces precracked at (a, c, e) 19.6 N and (b, d, f) 98 N by a Knoop indentor: (a, b) monolithic $BaTiO_3$, (c, d) $BaTiO_3$–1 vol% SiC, and (e, f) $BaTiO_3$–5 vol% SiC.

As the liquid-formation temperature of $Ba_2TiSi_2O_8$ phase is about 1400 °C [23], it is supposed that the grains grow exaggeratedly together with the formation of liquid $Ba_2TiSi_2O_8$ phase. At the same time, hexagonal $BaTiO_3$ started to appear as the major phase, as shown in Table I. In fact, hexagonal $BaTiO_3$ is a stable phase above 1430 °C [24]. On the other hand, the exaggerated grain growth could be depressed by further addition of the SiC particulate, therefore, the grain structure change with respect to the sintering temperature disappeared for the composite with 3 and 5 vol % SiC.

4.2. Mechanical properties

The fracture strength was remarkably affected by the sintering temperature and the relative density. The initial increase of the strength when sintered below 1300 °C, as observed in Fig. 7 for monolithic $BaTiO_3$, must be due to the relative density improvement. Thereafter the strength decreases with increasing sintering temperature. This result may be due to the abnormal grain growth or the spontaneous cracking, as can be seen in Fig. 3d and e. On the other hand, a sudden fracture strength decrease for 1 and 3 vol % SiC composites sintered at 1400 °C may be associated

with the appearance of the hexagonal phase and the resulting bimodal grain structure, as shown in Table I and discussed in Section 4.1.

The remarkable fracture-strength improvement by the incorporation of the SiC, as summarized in Table I, is mainly caused by the reduction in the grain size. In addition, the increases in the fracture toughness, Young's modulus and other mechanical properties, are thought to be other reasons for the observed fracture-strength improvement. Fracture-toughness increase may be caused by the SiC particulates. As can be seen in Table I, the measured micro-hardness and Young's modulus values are considerably higher than those expected from the Rule of mixture [17]. Similar results were reported by Yamamoto *et al.* [25]. It is concluded, therefore, that the enhancement of the fracture strength and Young's modulus are caused by the crystal structure variation which is associated with the nanosized SiC.

The strength difference below and above T_c observed in Fig. 8 is also caused by the internal stress [10, 11]. In the present study, the strength difference is directly proportional to the crystal structure variation with the SiC content. In other words, the crystal structure gradually changed from the tetragonal to cubic phase by the incorporation of SiC [15], and resulted in the decreasing strength difference with the SiC content. However, the reason why the fracture-strength difference for 1 vol % SiC composite is higher than that of the monolithic $BaTiO_3$ with much higher internal stresses, should be concerned with the difference in the stress relationship caused by the domain structure and elastic constant change with and without the SiC dispersions.

4.3. Fractography and SCG phenomenon

From the fracture surface observation, the fracture mode was found to be mainly intragranular regardless of the sintering temperature and SiC content. At the fracture origin and around it, however, intergranular fracture was observed for monolithic $BaTiO_3$ and 1 vol % SiC composite (Fig. 6). Further observation of fractured surfaces after CSF revealed that both the surface flaw produced by a Knoop indentor and the subsequent catastrophic (brittle) fracture, were intragranular, while, in the boundary region the intergranular fracture appeared together with the intragranular fracture. These observations suggest that the flaw grows subcritically before the catastrophic (fast) fracture occurs for the monolithic $BaTiO_3$ and $BaTiO_3$–1 vol % SiC composite.

Because the SCG phenomenon can be the origin of the catastrophic fracture and can reduce the lifetime at operating conditions, it is very important to investigate this phenomenon in electroceramics. In addition, the fracture strength of $BaTiO_3$ with a surface flaw produced by a Knoop indentor decreased gradually as the surface flaw grew under constant loading. Therefore, it is suggested that the fracture strength improvement of $BaTiO_3$–SiC composites may be partly caused by the depression of the SCG by the incorporation of SiC. Details of the SCG phenomenon in $BaTiO_3$ ceramics are described elsewhere [26].

5. Conclusions

1. The SiC particulates were uniformly distributed within the matrix $BaTiO_3$ grains, with some larger particulates located at the $BaTiO_3$ grain boundaries. The microstructure of $BaTiO_3$ was modified by incorporating the SiC particulate. It was confirmed that the added SiC particulate depressed the grain-boundary movement of $BaTiO_3$, and the grain size decreased with increasing SiC content.

2. The fracture strength of $BaTiO_3$ was increased markedly by the incorporation of nanosized SiC particulates. This observed fracture-strength improvement was mainly caused by the reduction in grain size of the $BaTiO_3$ matrix and also by the increase in fracture toughness and Young's modulus by the incorporation of SiC.

3. Young's modulus and micro-hardness strongly depended both on the dispersed SiC and the crystal structural variation of matrix caused by it.

4. The SCG phenomenon was observed for the monolithic $BaTiO_3$ before the catastrophic fracture occurred. The intergranular fracture appeared, together with intragranular fracture in the SCG region. It is thought that the depression of the SCG phenomenon by SiC addition is another reason for fracture-strength improvement of $BaTiO_3$–SiC composites.

References

1. A. F. DEVONSHIRE, *Philos. Mag.* **40** (1949) 1040.
2. W. R. BUESSEM, L. E. CROSS and A. K. GOSWAMI, *J. Am. Ceram. Soc.* **49** (1966) 32.
3. R. F. COOK, B. R. LAWN and C. J. FAIRBANKS, *ibid.* **68** (1985) 604.
4. K. OKAZAKI, *Am. Ceram. Soc. Bull.* **63** (1984) 1150.
5. S. K. NAG and D. C. AGRAWAL, *J. Mater. Sci* **27** (1992) 4125
6. H. NIITSUMA, T. TANAKA, N. CHUBACHI and R. SATO, *Jpn J. Appl. Phys.* **20** Suppl. 20–4 (1981) 193.
7. Q. JIANG, W. CAO and L.E. CROSS, *J. Am. Ceram. Soc.* **77** (1994) 211.
8. T. YAMAMOTO, H. IGASHIRA and K. OKAZAKI, *Ferroelectrics* **63** (1985) 281.
9. B. MALIC, M. KOSEC and T. KOSMAC, *ibid.* **129** (1992) 147.
10. R. C. POHANKA, S. W. FREIMAN and R. W. RICE, *ibid.* **28** (1980) 337.
11. R. C. POHANKA, S. W. FREIMAN and B. A. BENDER, *J. Am. Ceram. Soc.* **61** (1978) 72.
12. J. G. BRUCE, W. W. GERHERICH and B. G. KOEPKE, in "Fracture Mechanics of Ceramics," Vol 4, edited by R. C. Bradt, A. G. Evans, D. P. H. Hasselman and F. F. Lange (Plenum Press, New York, 1985) pp. 687–709.
13. J. M. BLAMEY and T. V. PARRY, *J. Mater. Sci.* **28** (1993) 4311.
14. *idem. ibid.* **28** (1993) 4317.
15. H. J. HWANG, T. SEKINO, K. OTA and K. NIIHARA, *ibid.* **31** (1996) 4617.
16. J. J. PETROVIC and M. G. MENDIRATTA, in "Fracture Mechanics Applied to Brittle Materials," edited by S. W. Frieman, ASTM STP 678 (American Society for Testing and Materials, Philadelphia, PA, 1979) p. 83.

17. W. D. KINGERY, H. K. BOWEN and D. R. UHLMANN, "Introduction to Ceramics" (Wiley, New York, 1976) p. 457
18. F. F. LANGE and M. M. HIRLINGER, *J. Am. Ceram. Soc.* **67** (1984) 164.
19. M. F. ASHBY and R. M. A. CENTAMORE, *Acta Metall.* **16** (1968) 1081.
20. R. W. RICER and R. C. POHANKA, *J. Am. Ceram. Soc.* **62** (1979) 559.
21. B. K. MOLNAR and R. W. RICE, *Am. Ceram. Soc. bull.* **52** (1973) 505
22. D. F. K. HENNINGS, R. JANSSEN and P. J. L. REYNEN, *J. Am. Ceram. Soc.* **70** (1987) 23.
23. Y. ITO, K. NAGATSUMA and S. ASHIDA, *Jpn J. Appl. Phys.* **20** Suppl. 20–4 (1981) 163
24. K. W. KIRBY and B. A. WECHSLSER, *J. Am. Ceram. Soc.* **74** (1991) 1841.
25. T. YAMAMOTO, H. IGARASHI and K. OKAZAKI, *ibid.* **66** (1983) 365.
26. H. J. HWANG, A. NAKAHIRA, T. SEKINO and K. NIIHARA, *J. Jpn Soc. Powder Powder Metall.* **41** (1994) 1175.

Received 1 December 1994
and accepted 13 February 1995